Periodic Trajectory Planning Beyond the Static Workspace for 6-DOF Cable-Suspended Parallel Robots

Xiaoling Jiang, Eric Barnett, and Clément Gosselin, *Fellow, IEEE*

***Abstract*—This paper proposes a dynamic trajectory planning technique for six-degree-of-freedom (6-DOF) cable-suspended parallel robots (CSPRs). First, a passive mechanical system that is equivalent to the CSPR is introduced to provide insight and facilitate the design of trajectories that can extend beyond the robot's static workspace. The tilt-and-torsion angle convention is used to develop the mathematical model and impose restrictions for the rotational component of the trajectories. The dynamic differential equations that govern the translational component of the trajectories are shown to become linear under some conditions. Natural frequencies of an equivalent passive linear system of constant-stiffness springs are, thus, obtained and the set of linear differential equations associated with this system is integrated to produce a general solution for natural, periodic trajectories. This approach is used to produce pure translation trajectories and more complex motion that includes changes in position and orientation. An experimental implementation is also presented using a 6-DOF prototype and a supplementary video file is included to demonstrate the results.**

***Index Terms*—Dynamic trajectory planning, six-degree-of-freedom (6-DOF) cable-suspended parallel robots (CSPRs), zero-moment trajectories.**

Manuscript received May 3, 2017; revised October 13, 2017; accepted February 5, 2018. Date of publication April 19, 2018; date of current version August 15, 2018. This paper was recommended for publication by Associate Editor M. Schwager and Editor I.-M. Chen upon evaluation of the reviewers' comments. This work was supported in part by the Natural Sciences and Engineering Research Council of Canada (NSERC), in part by the Canada Research Chair Program, and in part by the China Scholarship Council (CSC) through a scholarship to the first author. *(Corresponding author: Clément Gosselin.)*

X. Jiang is with the Faculty of Mechanical Engineering and Automation, Zhejiang Sci-Tech University, Hangzhou 310018, China, and also with the Department of Mechanical Engineering, Université Laval, Québec QC G1V 0A6, Canada (e-mail: xiaoling.jiang.1@ulaval.ca).

E. Barnett is with the Department of Mechanical Engineering, Université Laval, Québec QC G1V 0A6, Canada, and also with Robotiq, Lévis, QC G7A 2N1, Canada (e-mail: eric.barnett.1@ulaval.ca).

C. Gosselin is with the Department of Mechanical Engineering, Université Laval, Québec QC G1V 0A6, Canada (e-mail: gosselin@gmc.ulaval.ca).

This paper has supplementary downloadable material available at http://ieeexplore.ieee.org, video that shows the experimental prototype following several trajectories. Initially, the platform is moved slowly in a horizontal direction until one of the cables is clearly sagging, thereby showing the approximate edge of the static workspace. Then, a natural trajectory associated with constant-stiffness springs is shown, followed by an extended trajectory associated with variable-stiffness springs. Both trajectories involve variable position and orientation of the platform.

Color versions of one or more of the figures in this paper are available online at http://ieeexplore.ieee.org.

Digital Object Identifier 10.1109/TRO.2018.2819668

I. Introduction

CABLE-SUSPENDED parallel robots (CSPRs) are a class of cable-driven parallel robots (CDPRs) for which cable tension is generated by gravity. The first commercial application of CSPRs was the Skycam, which is a large CSPR that is typically positioned above a stadium for filming sporting events and other performances [1]. In industry, the NIST RoboCrane [2], with six controllable degrees of freedom (DOF), was proposed for stabilizing crane loads. More recently, CSPRs have been applied in the development of very large radio telescopes, such as the 500-m aperture spherical radio telescope [3] developed in China.

For many robotic systems, trajectory planning can be accomplished by considering only kinematic and geometric constraints. However, for CSPRs, dynamic constraints must also be considered in most cases, due to the unilateral tension property of cables.

Several techniques have been proposed for the CSPR trajectory planning. In [4], wrench-feasible trajectories were designed for cable-driven hexapods. In [5]–[7], trajectories were planned to minimize the time required to follow fully specified paths. Some of these techniques adapted a trajectory planning approach developed for serial manipulators [8]–[10]. Elsewhere, the dynamic load-carrying capacity defined in [11] was taken into account in the formulation of optimal trajectories for CSPRs [12], [13].

In [14] and [15], a dynamic trajectory planning approach for point-mass CSPRs was developed, which globally guarantees that cables remain tensioned and does not need to verify or impose tension constraints *locally* along the trajectory. A series of periodic trajectories were defined parametrically as analytic functions of time, revealing the existence of certain oscillation frequencies for which the equations of motion become linear, with constant ratios between the force and length for each cable. This approach greatly reduces the complexity of algebraic cable tension calculations and allows for the design of periodic trajectories that can always be feasible, with theoretically unbounded amplitude. Since these dynamic trajectories can extend beyond the static workspace of the robot, they can potentially be used for many new CSPR applications.

There are several examples of prior work involving dynamic trajectories for 3-DOF point-mass CSPRs that can go beyond the static workspace. In [16], a user-friendly approach was proposed to extend and control the dynamic trajectories designed

in [14] and [15]. In [17] and [18], a geometry-based trajectory planning approach was introduced, with periodic linear and circular trajectories designed in the position-acceleration phase plane.

For most of the prior work on dynamic trajectory planning for CSPRs, the dynamic equations governing the motion of cable robots are used as constraints that can keep the cables under tension [14]–[17]. However, in [19], dynamic trajectories were directly obtained from the integration of the dynamic equations for 3-DOF planar CSPRs. The results obtained there for the translational component generalized the harmonic trajectories obtained in [14] and [15] and highlighted the critical role that special oscillation frequencies play in the dynamic equations.

In [20], it was shown that each special oscillation frequency found in the earlier work is equivalent to the natural frequency of a mass–spring oscillator, with the ratio between cable force and length being the equivalent spring stiffness. A 3-DOF CSPR can, thus, be modeled as a linear system of three mass–springs that exhibits 3-D undamped harmonic oscillation if the spring stiffnesses are constant. Oscillation in different directions can be used to produce linear, circular, and elliptical trajectories. However, variable stiffness trajectories were not addressed in [19] and [20] and rotational trajectory planning is still a challenge.

In this paper, dynamic trajectories are produced for fully actuated 6-DOF CSPRs based on the analytical integration of the dynamic equations. Here, the term *dynamic* refers to the fact that the trajectories can extend beyond the static workspace of the robot. Natural frequencies of an equivalent linear system are obtained and a generalization of the associated natural dynamic trajectories is accomplished by the integration of the translational component of the dynamic equations, which reduces to a linear system of differential equations. Natural trajectories are defined as trajectories associated with constant-stiffness springs and with no bounds on the amplitudes, which are a class of linear trajectories corresponding to the linear system of differential equations. Extended trajectories associated with variable-stiffness springs are also obtained, including pure translational linear trajectories and combined trajectories that involve changes in both position and orientation. Cable tension constraints are imposed directly, rather than by substituting trajectories into the dynamic equations.

In Section II, the kinematic and dynamic models of the mechanism are presented and the vibration model of an equivalent passive system is introduced as a tool to help analyze the mechanism. Section III introduces the conditions that define pure translational trajectories and combined motions. In Section IV, the trajectories obtained in Section III are applied to a specific robot architecture. Finally, an experimental prototype is used to validate the proposed technique, as shown in the supplementary video file.

II. Mechanics of 6-DOF CSPRs

In this section, the equations that govern the kinematics and dynamics of 6-DOF CSPRs are first formulated. Then, the dynamic equations of an equivalent freely vibrating undamped system are derived. Finally, the differential equations of motion of this equivalent system are developed.

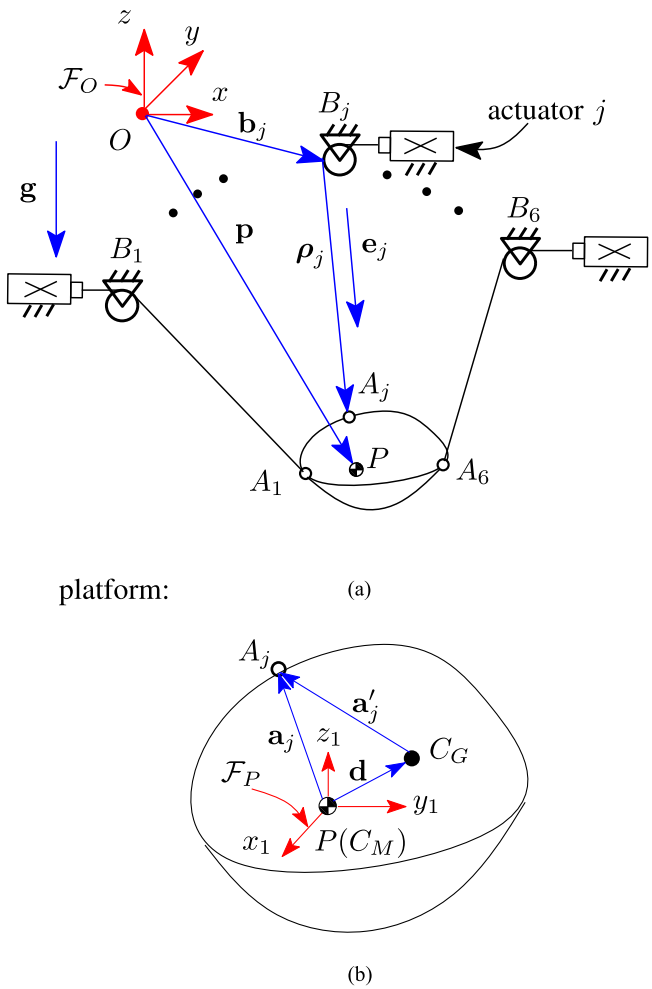

Fig. 1. Geometric parameters of a 6-DOF CSPR.

A. Robot Architecture

A general six-DOF CSPR is represented schematically in Fig. 1. Six actuated spools mounted on a fixed structure are used to control the extension of the cables, which are assumed to be massless and inelastic. Each cable is assumed to pass through a guide such as an eyelet before extending downward in a straight line to an attachment point on the robot end effector, which is referred to as the moving platform. The robot has six actuators and six degrees of freedom and is, therefore, fully actuated, capable of controlling both the position and orientation of the platform. However, since cable transmission is unilateral and cables can become slack, the platform is not fully constrained.

B. Kinematic and Dynamic Modeling

A fixed reference frame $\mathcal{F}_O$ with origin O is defined on the base of the robot, as illustrated in Fig. 1. The z-axis of the fixed reference frame points upwards, opposite to the direction of gravity. Point B_j, with $j = 1, \ldots, 6$, is fixed and corresponds to the location where cable j exits its pulley or eyelet. In the

following, indices j should be assumed to go from 1 to 6 and a plural form of an item h_j is denoted $\{h_j\}_1^6$, unless specified otherwise. The vector $\mathbf{b}_j$ connects origin O to point B_j.

A moving reference frame $\mathcal{F}_P$ is located on the platform, with its origin P located at the center of mass of the robot C_M. Vector $\mathbf{a}_j$ goes from P to cable attachment point A_j, which is on the platform but not otherwise constrained. Point C_G is the geometric center of the attachment points $\{A_j\}_1^6$ on the platform. The vector $\mathbf{d}$ connects C_M to point C_G and vector $\mathbf{a}'_j$ connects C_G to point A_j. Position vector $\mathbf{p} = [x, y, z]^T$ expresses the position of C_M with respect to O.

The inverse kinematic equations can be written as

$$\boldsymbol{\rho}_j = \mathbf{p} + \mathbf{Q}\mathbf{a}_j - \mathbf{b}_j \tag{1}$$

where $\boldsymbol{\rho}_j$ is the vector connecting point B_j to point A_j along the jth cable, $\mathbf{Q}$ is the rotation matrix from $\mathcal{F}_O$ to $\mathcal{F}_P$, and ρ_j is the effective cable length, given by

$$\rho_j = \sqrt{(\mathbf{p} + \mathbf{Q}\mathbf{a}_j - \mathbf{b}_j)^T(\mathbf{p} + \mathbf{Q}\mathbf{a}_j - \mathbf{b}_j)}.$$

Finally, $\mathbf{e}_j = \boldsymbol{\rho}_j/\rho_j$ is defined as the unit vector in the direction of the jth cable, oriented from B_j to A_j.

The dynamic model of the platform is built using the Newton–Euler approach, which yields

$$\sum_{j=1}^{6}\left(\frac{-f_j}{\rho_j}\boldsymbol{\rho}_j\right) + m\mathbf{g} = m\ddot{\mathbf{p}} \tag{2}$$

$$\sum_{j=1}^{6}(\mathbf{Q}\mathbf{a}_j) \times \left(-\frac{f_j}{\rho_j}\boldsymbol{\rho}_j\right) = \mathbf{Q}(\mathbf{I}\dot{\boldsymbol{\omega}} + \boldsymbol{\omega} \times \mathbf{I}\boldsymbol{\omega}) \tag{3}$$

where m is the platform mass, $\mathbf{I}$ is the inertia tensor of the platform, $\ddot{\mathbf{p}}$ is the acceleration of the center of mass, $\boldsymbol{\omega}$ and $\dot{\boldsymbol{\omega}}$ are, respectively, the angular velocity and angular acceleration of the platform with respect to the moving reference frame $\mathcal{F}_P$, f_j is the tension in the jth cable, and $\mathbf{g} = [0, 0, -g]^T$ is the vector of gravitational acceleration.

Equations (2) and (3) can be written in matrix form as

$$\mathbf{M}\mathbf{k} = \boldsymbol{\gamma} \tag{4}$$

where

$$\boldsymbol{\gamma} = \begin{bmatrix} m(\mathbf{g} - \ddot{\mathbf{p}}) \\ \mathbf{Q}(\mathbf{I}\dot{\boldsymbol{\omega}} + \boldsymbol{\omega} \times \mathbf{I}\boldsymbol{\omega}) \end{bmatrix} \tag{5}$$

$$\mathbf{k} = \begin{bmatrix} k_1 & k_2 & k_3 & k_4 & k_5 & k_6 \end{bmatrix}^T, \quad k_j = \frac{f_j}{\rho_j} \tag{6}$$

and

$$\mathbf{M} = \begin{bmatrix} \boldsymbol{\rho}_1 & \cdots & \boldsymbol{\rho}_6 \\ (\boldsymbol{\rho}_1 \times \mathbf{Q}\mathbf{a}_1) & \cdots & (\boldsymbol{\rho}_6 \times \mathbf{Q}\mathbf{a}_6) \end{bmatrix} \tag{7}$$

where $\mathbf{k}$ is the vector of cable tension-to-length ratios, whose components must all remain positive to ensure that the cables remain taut. The vector $\boldsymbol{\tau}$ of cable tensions is then written as

$$\boldsymbol{\tau} = \begin{bmatrix} k_1\rho_1 & k_2\rho_2 & k_3\rho_3 & k_4\rho_4 & k_5\rho_5 & k_6\rho_6 \end{bmatrix}^T. \tag{8}$$

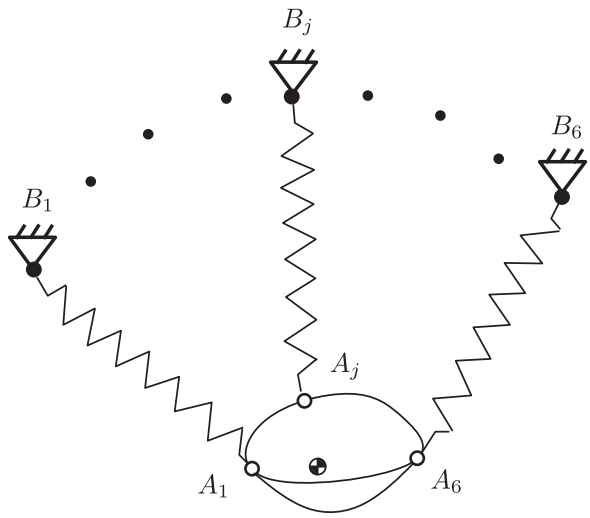

Fig. 2. Virtual equivalent mass–spring system for a 6-DOF CSPR.

C. Vibration Model of a Passive Equivalent System

等效无阻尼质量-弹簧系统

A CSPR can be treated as a set of undamped mass–springs to gain insight into its behavior and facilitate trajectory planning. Indeed, each of the actuator-cable modules can be replaced by a corresponding spring of stiffness k_j, and therefore, the complete system can be modeled as a platform suspended by six springs, as illustrated in Fig. 2.

Applying (1)–(3) and (6), the dynamic equations for the system of Fig. 2 can be written as

$$\begin{aligned} m\ddot{\mathbf{p}} &= \mathbf{f}_{\text{res}} + m\mathbf{g} \\ &= -\sum_{j=1}^{6} k_j(\mathbf{p} + \mathbf{Q}\mathbf{a}_j - \mathbf{b}_j) + m\mathbf{g} \end{aligned} \tag{9}$$

and

$$\begin{aligned} &\mathbf{Q}(\mathbf{I}\dot{\boldsymbol{\omega}} + \boldsymbol{\omega} \times \mathbf{I}\boldsymbol{\omega}) \\ &\quad= \sum_{j=1}^{6} k_j(\mathbf{p} + \mathbf{Q}\mathbf{a}_j - \mathbf{b}_j) \times \mathbf{Q}\mathbf{a}_j \\ &\quad= \sum_{j=1}^{6} k_j(\mathbf{p} - \mathbf{b}_j) \times \mathbf{Q}\mathbf{a}_j \end{aligned} \tag{10}$$

where $\mathbf{f}_{\text{res}}$ is the resultant cable force and k_j is the stiffness of the jth equivalent spring, referred to simply as the stiffness below. Each spring has zero free length, i.e., the force in the jth spring is zero if ρ_j is equal to zero. Additionally, the sum of spring stiffnesses is defined as

$$K = \sum_{j=1}^{6} k_j. \tag{11}$$

The purpose of this passive model is to guide trajectory planning for the active robot. Indeed, if natural free-motion trajectories of the passive system can be found, it can be guaranteed that these trajectories can be performed by the active robot while

maintaining the cables in tension, as long as the actuator torque and velocity limits are respected.

III. Trajectory Planning

The dynamic model developed in Section II can be used to simulate the robot behavior along any trajectory. Here, this model is linearized, and then, a procedure is introduced for generating natural trajectories, which are defined as trajectories generated from a linearized dynamic model that has a passive equivalent system with constant-stiffness springs.

To provide insight into the fundamental properties of 6-DOF CSPRs, natural trajectories are designed for pure translation, and then, for combined motion, which involves changes in both position and orientation. Constant spring stiffnesses $\{k_{sj}\}_1^6$ are used instead of $\{k_j\}_1^6$ and the *constant* total stiffness is given by

$$K_s = \sum_{j=1}^{6} k_{sj}. \tag{12}$$

这样的跟随运动，能保证张力恒为正

If such motions are then followed by the robot, it can be guaranteed that the cable tensions will be positive at all times because the spring forces of the passive free vibrating system are positive at all times.

Although natural trajectories are interesting from a fundamental perspective, trajectories associated with variable-stiffness springs are much less restrictive on the type of motion that can be performed. Section IV-C introduces a variable-stiffness trajectory planning approach that greatly expands the range of feasible trajectories for the 6-DOF CSPR prototype.

A. Pure Translation

For pure translation trajectories, the fixed and moving frames are always in the same orientation, i.e., $\mathbf{Q} = \mathbf{1}$, the identity matrix. Additionally, $\boldsymbol{\omega} = \dot{\boldsymbol{\omega}} = \mathbf{0}$, which leads to

$$\mathbf{I}\dot{\boldsymbol{\omega}} + \boldsymbol{\omega} \times \mathbf{I}\boldsymbol{\omega} = \mathbf{0}. \tag{13}$$

Considering this result and (10), two sufficient conditions for pure translation are then

$$\sum_{j=1}^{6} k_j \mathbf{p} \times \mathbf{a}_j = \mathbf{p} \times \sum_{j=1}^{6} k_j \mathbf{a}_j = \mathbf{0} \tag{14}$$

and

$$\sum_{j=1}^{6} k_j \mathbf{b}_j \times \mathbf{a}_j = \mathbf{0}. \tag{15}$$

Equation (14) implies that vector $\sum_{j=1}^{6} k_j \mathbf{a}_j$ is aligned with vector $\mathbf{p}$, i.e.,

$$\sum_{j=1}^{6} k_j \mathbf{a}_j = H\mathbf{p} \tag{16}$$

with H being a scalar multiplication factor.

Substituting (16) and $\mathbf{Q} = \mathbf{1}$ into (9), the translational component of the dynamic equations can be written as

$$m\ddot{\mathbf{p}} + K_H \mathbf{p} - \sum_{j=1}^{6} k_j \mathbf{b}_j - m\mathbf{g} = \mathbf{0} \tag{17}$$

with $K_H = K + H$, where K is defined in (11) and H is seen as the stiffness of a virtual spring, which is not associated with a particular cable but arises to respect the moment-component coupling in (14).

If the cable attachment points $\{B_j\}_1^6$ are in a plane at the same height and the origin of fixed frame $\mathcal{F}_O$ lies in this plane, the z-component of each vector $\mathbf{b}_j$ is zero. The last row of (17) can then be written as

$$K_H = \frac{-m\,(g + \ddot{z})}{z}. \tag{18}$$

Furthermore, K_H is constant when z undergoes simple harmonic motion, according to

$$z = z_s + z_d \tag{19}$$

with

$$z_s = -g/\omega_n^2, \quad z_d = \mu_{zc} \cos \omega_n t + \mu_{zs} \sin \omega_n t \tag{20}$$

where $z_s < 0$ is the central static equilibrium position on the z-axis. The constant parameters μ_{zc} and μ_{zs} determine the amplitude of the motion, and since these parameters are *unbounded*, the end effector can go *above* the cable attachment points $\{B_j\}_1^6$.

In practice, trajectories that extend above $\{B_j\}_1^6$ impose many significant restrictions on the CSPR design. In fact, for the 6-DOF mechanism considered herein, such trajectories are not possible as they would result in cable interference. Therefore, only trajectories for which $z < 0$ are considered below, ensuring that the mechanism remains *suspended*. Trajectories above $\{B_j\}_1^6$ were achieved in [17] and [18] for a point-mass CSPR.

Substituting (19) into the right-hand side of (18) yields

$$K_H = m\omega_n^2. \tag{21}$$

Under these circumstances, the nonlinear differential equation (17) simplifies to

$$m\ddot{\mathbf{p}} + m\omega_n^2 \mathbf{p} - \sum_{j=1}^{6} k_j \mathbf{b}_j - m\mathbf{g} = \mathbf{0} \tag{22}$$

which can be readily integrated when the term $\sum_{j=1}^{6} k_j \mathbf{b}_j$ is a constant force vector $\mathbf{w}$, i.e., when

$$\sum_{j=1}^{6} k_j \mathbf{b}_j = \mathbf{w}. \tag{23}$$

Since $\mathbf{b}_j$ is a constant vector from the origin of the fixed frame to the fixed cable attachment point B_j, condition (23) is satisfied when each cable stiffness k_j is constant; it can also be satisfied for variable k_j if some additional restrictions are placed on vectors $\{\mathbf{b}_j\}_1^6$, as will be seen in Section IV.

The linearized version of (22) is the system of three second-order differential equations

$$\ddot{\mathbf{p}} + \omega_n^2 \mathbf{p} - (\mathbf{v} + \mathbf{g}) = \mathbf{0} \tag{24}$$

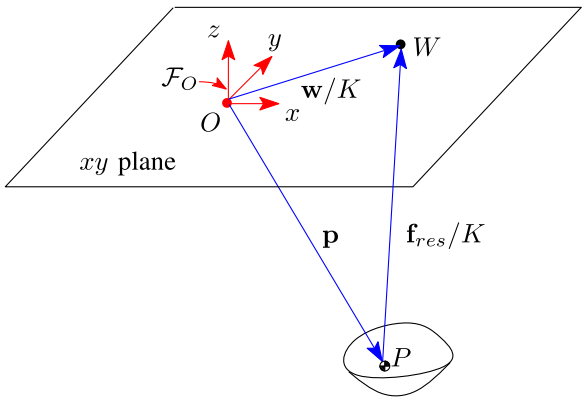

Fig. 3. Resultant cable force $\mathbf{f}_{\text{res}}$ points toward W, which is located in the xy plane.

where $\mathbf{v} = [v_1, v_2, 0]^T = \mathbf{w}/m$ is constant. The last element of vector $\mathbf{v}$ is zero if the z-component of each vector $\mathbf{b}_j$ is zero, i.e., if points $\{B_j\}_1^6$ and O are in the same horizontal plane. Physically, (24) describes an undamped harmonic oscillator, and (9), (16), (18), and (23) can be combined to obtain the resultant cable force

$$\begin{aligned}\mathbf{f}_{\text{res}} &= -\sum_{j=1}^{6} k_j(\mathbf{p} + \mathbf{a}_j - \mathbf{b}_j) \\ &= -\left(\sum_{j=1}^{6} k_j + H\right)\mathbf{p} + \mathbf{w} \\ &= -K_H\mathbf{p} + \mathbf{w}.\end{aligned}$$

This force is parallel to the vector that goes from the platform center of mass to the fixed point W, which is the point in the xy plane located at the tip of position vector $\mathbf{w}/K$, which is shown in Fig. 3. In particular, if $\mathbf{w} = \mathbf{0}$, $\mathbf{f}_{\text{res}}$ points in the opposite direction as $\mathbf{p}$, i.e., from P toward O.

The translational component of the trajectories can be obtained by analytically integrating (24) to obtain

$$\mathbf{p} = \mathbf{p}_d + \mathbf{p}_s \tag{25}$$

with

$$\mathbf{p}_s = [x_s, y_s, z_s]^T = \left[\frac{v_1}{\omega_n^2}, \frac{v_2}{\omega_n^2}, -\frac{g}{\omega_n^2}\right]^T \tag{26}$$

and

$$\mathbf{p}_d = \mathbf{c}\cos\omega_n t + \mathbf{s}\sin\omega_n t \tag{27}$$

where the natural frequency is

$$\omega_n = \sqrt{\frac{K_H}{m}} \tag{28}$$

$\mathbf{c} = [\mu_{xc}, \mu_{yc}, \mu_{zc}]^T$ and $\mathbf{s} = [\mu_{xs}, \mu_{ys}, \mu_{zs}]^T$. Geometrically, $\mathbf{p}_s$ represents the central static equilibrium position, which should be located in the robot static workspace, and $\mathbf{c}$ and $\mathbf{s}$ are design parameters that determine the shape of the motion.

1) Natural Pure Translation: Since each vector $\mathbf{a}_j$ is constant, (14) yields the condition

$$\sum_{j=1}^{6} k_{sj}\mathbf{a}_j = \mathbf{0} \tag{29}$$

which in turn implies that $H = 0$ is a solution for (16). Alternatively, $\mathbf{p}$ could be aligned with the constant vector $\sum_{j=1}^{6} k_{sj}\mathbf{a}_j$ to satisfy (16), but this would only allow for trajectories which oscillate along the direction of this vector. Equation (29) also implies that the convex hull defined by the attachment points on the platform includes the center of mass, since each spring stiffness k_{sj} must be positive.

When the passive system is in static equilibrium, (9), (10), and (29) can be combined to obtain

$$\sum_{j=1}^{6} k_{sj}\mathbf{b}_j + m\mathbf{g} = K_s\mathbf{p}_s \tag{30}$$

$$\sum_{j=1}^{6} k_{sj}\mathbf{b}_j \times \mathbf{a}_j = \mathbf{0}. \tag{31}$$

Then, substituting (25), (30), (31), and $\mathbf{Q} = \mathbf{1}$ into the dynamic equations (9) and (10), the free vibration model of the linear system can be obtained, namely

$$m\ddot{\mathbf{p}}_d + K_s\mathbf{p}_d = \mathbf{0} \tag{32}$$

$$\mathbf{p}_d \times \sum_{j=1}^{6} k_{sj}\mathbf{a}_j = \mathbf{0} \tag{33}$$

where $\mathbf{p}_d = \mathbf{p} - \mathbf{p}_s$, i.e., $\mathbf{p}_d$ represents the displacement from the equilibrium position. The solution to (32) has the same form as (27) and the static equilibrium position $\mathbf{p}_s = [x_s, y_s, -g/\omega_n^2]^T$ can be obtained from (30) and (31). The natural frequency ω_n is obtained from (28). The two sufficient conditions for pure translation (14) and (15) are satisfied by inspection of (29) and (31).

Under these conditions, when $\mathbf{p}_d$ is defined according to (27) and $\mathbf{p}_s$ is located in the static workspace, it can be guaranteed that the tensions in the cables will remain positive because the equivalent spring stiffnesses are always positive.张力恒正

During these trajectories, when (29) is applied, the resultant cable force becomes

$$\mathbf{f}_{\text{res}} = -\sum_{j=1}^{6} k_{sj}(\mathbf{p} - \mathbf{b}_j) = -K_s\mathbf{p} + \mathbf{w}. \tag{34}$$

B. Combined Motion

The dynamics equations (9) and (10) are considered once more for the design of combined motion, which involves variable position and orientation. When the conditions

$$\sum_{j=1}^{6} k_j\mathbf{b}_j \times \mathbf{Q}\mathbf{a}_j = \mathbf{0} \tag{35}$$

and

$$\sum_{j=1}^{6} k_j \mathbf{b}_j = \mathbf{0} \tag{36}$$

are imposed, and the vector equation $\mathbf{a}_j = \mathbf{a}'_j + \mathbf{d}$, shown schematically in Fig. 1, is considered, the dynamic equations can be greatly simplified to

$$m\ddot{\mathbf{p}} + K\mathbf{p} + K\mathbf{Q}\mathbf{d} + \mathbf{u} = m\mathbf{g} \tag{37}$$

and

$$\mathbf{Q}(\mathbf{I}\dot{\boldsymbol{\omega}} + \boldsymbol{\omega} \times \mathbf{I}\boldsymbol{\omega}) - K\mathbf{p} \times \mathbf{Q}\mathbf{d} = \mathbf{p} \times \mathbf{u} \tag{38}$$

where

$$\mathbf{u} = \mathbf{Q}\sum_{j=1}^{6} k_j \mathbf{a}'_j = [u_1, u_2, u_3]^T. \tag{39}$$

As long as $\mathbf{u}$ is obtained for a specific architecture and $\{k_j\}_1^6$ obtained from (35) and (36), trajectories can be generated from the differential equations (37) and (38). An example of a general case with variable $\mathbf{u}$ is provided in Section IV-C. Here, natural combined trajectories are designed to satisfy the condition $\mathbf{u} = \mathbf{0}$. This choice is makes the cable stiffnesses $\{k_j\}_1^6 = \{k_{sj}\}_1^6$ independent of the rotation matrix $\mathbf{Q}$, which greatly simplifies the dynamics equations. Indeed, with this choice, the stiffnesses depend only on m and ω, and the attachment points on the moving platform $\{\mathbf{a}'_j\}_1^6$.

1) Rotational Component: The rotational motion is described using the tilt-and-torsion (T&T) angle convention, which is a suitable approach for parallel mechanisms [21]. In this convention, ϕ represents the azimuth angle, θ is the tilt angle, and σ is the torsion angle. The rotational component is designed such that σ is set to zero to avoid cable tangling, θ is prescribed to be constant, and ϕ is designed to have constant angular velocity, according to

$$\sigma = \dot{\sigma} = \ddot{\sigma} = 0, \quad \theta = \theta_0, \quad \dot{\theta} = \ddot{\theta} = 0, \quad \dot{\phi} = \omega, \quad \ddot{\phi} = 0. \tag{40}$$

The tilt angle is restricted to the range $-\pi/2 < \theta_0 < \pi/2$ since the platform cannot flip.

The unit vector

$$\mathbf{s} = [\cos\phi,\ \sin\phi,\ 0]^T \tag{41}$$

represents the axis of rotation, with the rotation matrix corresponding to a rotation of angle $\theta = \theta_0$ around $\mathbf{s}$ then being

$$\mathbf{Q} = \mathbf{s}\mathbf{s}^T + \cos\theta_0(\mathbf{1} - \mathbf{s}\mathbf{s}^T) + \sin\theta_0\mathbf{S} \tag{42}$$

where $\mathbf{S}$ is the cross-product matrix of the vector $\mathbf{s}$. Upon expansion, one has

$$\mathbf{Q} = \begin{bmatrix} c_\phi^2 + c_0 s_\phi^2 & c_\phi s_\phi(1-c_0) & s_0 s_\phi \\ c_\phi s_\phi(1-c_0) & s_\phi^2 + c_0 c_\phi^2 & -s_0 c_\phi \\ -s_0 s_\phi & s_0 c_\phi & c_0 \end{bmatrix}$$

where $c_0 = \cos\theta_0$, $s_0 = \sin\theta_0$, $c_\phi = \cos\phi$, and $s_\phi = \sin\phi$. The rotational component in (4) and the unit vector $\mathbf{s}$ are illustrated in Fig. 4.

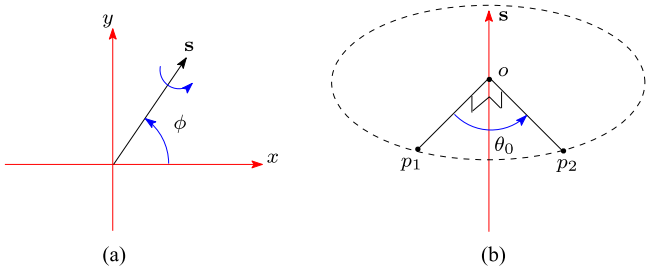

Fig. 4. Illustration of the rotational component trajectories defined in (40) and the unit vector $\mathbf{s}$.

The cross-product matrix $\boldsymbol{\Omega}_O$ of the vector $\boldsymbol{\omega}_O = \begin{bmatrix}\omega_{1O} & \omega_{2O} & \omega_{3O}\end{bmatrix}^T$, which is the angular velocity of the platform with respect to the fixed frame, is given by

$$\boldsymbol{\Omega}_O = \dot{\mathbf{Q}}\mathbf{Q}^T = \begin{bmatrix} 0 & -\omega_{3O} & \omega_{2O} \\ \omega_{3O} & 0 & -\omega_{1O} \\ -\omega_{2O} & \omega_{1O} & 0 \end{bmatrix}. \tag{43}$$

By inspecting Ω_O, the angular velocity $\boldsymbol{\omega}_O$ can be found. Then, using ω_O and the rotational component designed in (40), the angular velocity in the moving frame is found to be

$$\boldsymbol{\omega} = \mathbf{Q}^T\boldsymbol{\omega}_O = \omega\begin{bmatrix} -\sin\theta_0\sin\phi \\ \sin\theta_0\cos\phi \\ -1+\cos\theta_0 \end{bmatrix} \tag{44}$$

and the angular acceleration

$$\dot{\boldsymbol{\omega}} = -\omega^2\sin\theta_0\mathbf{s}. \tag{45}$$

With the assumption that $I_{xy} = I_{xz} = I_{yz} = 0$ and $I_{xx} = I_{yy}$ and substituting (42), (44), and (45) into the left-hand side of (10), the external moment on the C_M can be obtained as

$$\mathbf{Q}(\mathbf{I}\dot{\boldsymbol{\omega}} + \boldsymbol{\omega} \times \mathbf{I}\boldsymbol{\omega}) = c_w\mathbf{s} \tag{46}$$

where

$$c_w = \omega^2\sin\theta_0 c_I, \quad c_I = -I_{zz}(1-\cos\theta_0) - I_{xx}\cos\theta_0. \tag{47}$$

The constraints imposed on the elements of inertia tensor imply that if equipment such as a scanning/video system is mounted on the platform, it must be carefully located and/or counterbalanced.

Assuming that C_M is located at a distance d below C_G, i.e., $\mathbf{d} = [0, 0, d]^T$, with $\mathbf{Q}$ is defined according to (42), one has

$$\mathbf{Q}\mathbf{d} = -d\sin\theta_0\begin{bmatrix} -\sin\phi & \cos\phi & -\cot\theta_0 \end{bmatrix}^T \tag{48}$$

and

$$\mathbf{p} \times \mathbf{Q}\mathbf{d} = d\begin{bmatrix} y\cos\theta_0 + z\sin\theta_0\cos\phi \\ -x\cos\theta_0 + z\sin\theta_0\sin\phi \\ -\sin\theta_0(x\cos\phi + y\sin\phi) \end{bmatrix}. \tag{49}$$

2) Natural Combined Motion: With the constant stiffnesses $\{k_{sj}\}_1^6$ satisfying

$$\sum_{j=1}^{6} k_{sj}\mathbf{a}'_j = \mathbf{0} \tag{50}$$

(41) and (46) can be combined with the rotational dynamics equation (38) to obtain

$$c_w \mathbf{s} - K_s \mathbf{p} \times \mathbf{Qd} = \mathbf{0}. \tag{51}$$

Since the z-component of $\mathbf{s}$ is zero, if $d \neq 0$ and $\sin\theta_0 \neq 0$, the last rows of (49) and (51) can be combined to obtain

$$x \cos\phi + y \sin\phi = 0 \tag{52}$$

which describes a circle in the xy plane. The trajectory components in the x- and y-directions can be obtained as functions of z, namely

$$x = -\mu \sin\phi, \quad y = \mu \cos\phi \tag{53}$$

with

$$\mu = \left(\frac{\omega^2 c_I}{d K_s} - z \right) \tan\theta_0 \tag{54}$$

which satisfies (52). The coupled trajectory becomes

$$\phi = \omega t - \pi/2, \quad x = \mu \cos\omega t, \quad y = \mu \sin\omega t \tag{55}$$

or

$$\phi = \omega t + \pi/2, \quad x = \mu \cos\omega t, \quad y = -\mu \sin\omega t. \tag{56}$$

These two cases represent the same circular motion in opposite directions: counter-clockwise for (55) and clockwise for (56).

Next, the translational component of the dynamic equation (37) is combined with (48), (53), and (54) to produce

$$\begin{aligned} m\ddot{x} + K_n x &= 0 \\ m\ddot{y} + K_n y &= 0 \\ m\ddot{z} + K_s z &= -K_s d \cos\theta_0 - mg \end{aligned} \tag{57}$$

where

$$K_n = K_s \left(1 + \frac{d^2 K_s \cos\theta_0}{dz K_s - c_I \omega^2} \right). \tag{58}$$

Here, it is important to note that K_n has been defined to eliminate explicit dependence on ϕ in the differential equations for x and y. All three equations, thus, describe simple harmonic oscillators with frequencies that depend only on mechanism and trajectory design parameters. The stiffness parameter K_n is a positive constant if z is the constant z_s, and if the sufficient condition

$$z_s < \frac{c_I \omega^2}{d K_s} - d \cos\theta_0 \tag{59}$$

is satisfied. Therefore, trajectories in the x- and y-directions can be readily obtained by the integration of the first two linear differential equations in (57), which will match with (53) by choosing

$$\omega = \sqrt{\frac{K_n}{m}}.$$

From the third equation of (57), one obtains the restriction

$$z_s = -\frac{g}{\omega_n^2} - d \cos\theta_0 < 0 \tag{60}$$

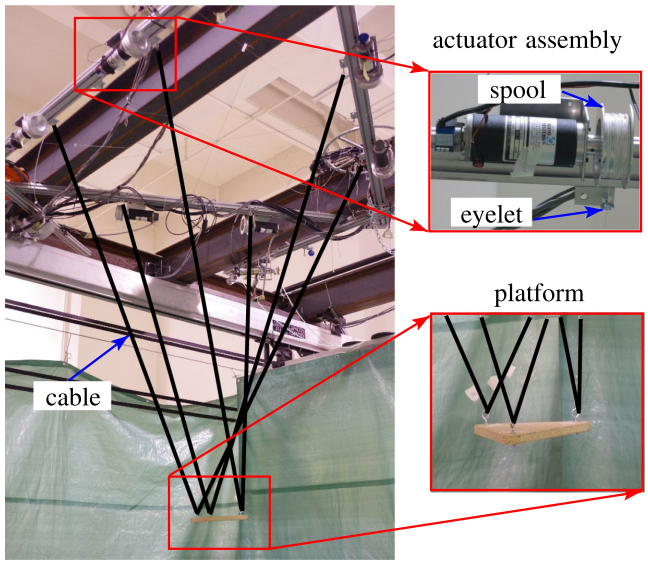

Fig. 5. 6-DOF cable-suspended parallel mechanism prototype.

with

$$\omega_n = \sqrt{\frac{K_s}{m}}. \tag{61}$$

In summary, natural combined motion is defined by a rotational component in (40) and a translational component given in (55) and (60), obtained through integration of the linear differential equations (57). Positive constant spring stiffnesses $\{k_{sj}\}_1^6$ can be obtained applying (12), (35), (36), (50), and (61) to a specific architecture, when z_s satisfying (59). Extended trajectories associated with variable stiffness springs are introduced in the next section, because the mathematical formulation becomes much simpler when certain assumptions are made about the mechanism geometry.

IV. Simulations with a Specific Robot Architecture

The experimental prototype shown in Fig. 5 is used to validate the proposed technique. Natural trajectories with constant stiffness springs $\{k_{sj}\}_1^6$ are planned first, for which the amplitude is not bounded. Then, trajectories associated with variable but positive stiffnesses $\{k_j\}_1^6$ are designed, including pure translations which are formed by integrating the linear system (24), and combined translational and rotational motions which arise directly from the dynamic equations (9) and (10).

The main benefit of the proposed approach is the ability to plan trajectories that extend beyond the static workspace of the robot. Although this workspace cannot be intuitively represented when orientation and position vary at the same time, it obviously lies within the hexagonal-prism-shaped volume formed when projecting the fixed-frame cable attachment points downward. In the supplementary video file, one edge of the static workspace is clearly shown by slowly commanding the robot to move in one direction, until a cable starts to sag. Later in the video, while following dynamic trajectories, the cables are clearly all taut when the platform is beyond this point. Therefore, the dynamic trajectories clearly exit the hexagonal-prism-shaped volume, so

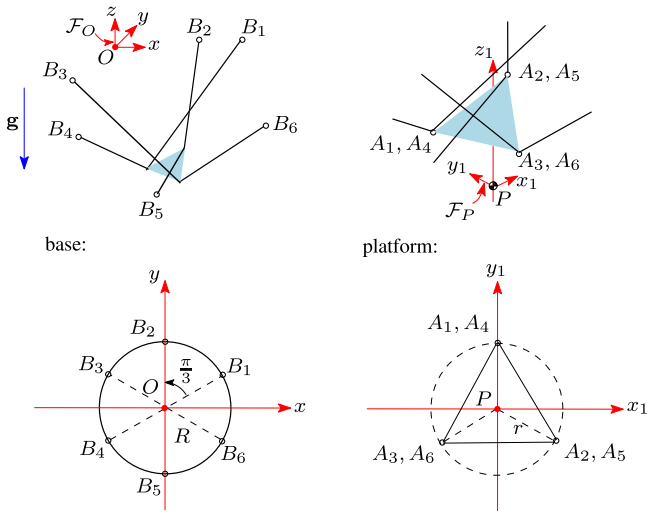

Fig. 6. Geometry of the cable attachment points for the 6-DOF CSPR prototype.

they must also exit the static workspace. In fact, the platform could have gone much further outside the static workspace had it not been for a few obstacles nearby.

A. Geometry of the Prototype

The architecture of the prototype is illustrated in Fig. 6. This geometry was proposed in [22], based on an optimization of the feasible workspace. Spools $\{B_j\}_1^6$ are evenly placed on a circle of radius $R = 0.68$ m. There are three attachment points on the moving platform, which form an equilateral triangle circumscribed by a circle of radius $r = 0.1$ m. Two cables are connected to each attachment point, as shown in Figs. 5 and 6. The center of mass C_M is located at a distance d below the geometric center of the platform attachment points C_G, i.e., $\mathbf{d} = [0, 0, d]^T$. The mass of the platform is $m = 0.316$ kg. The cable attachment point vectors are given by

$$\mathbf{b}_j = R\begin{bmatrix}\cos\beta_{bj} & \sin\beta_{bj} & 0\end{bmatrix}^T \tag{62}$$

$$\mathbf{a}_j = \begin{bmatrix}r\cos\beta_{aj} & r\sin\beta_{aj} & d\end{bmatrix}^T \tag{63}$$

with

$$\beta_{bj} = \frac{(j-1)\pi}{3} + \frac{\pi}{6}, \quad \beta_{aj} = -\frac{2(j-1)\pi}{3} + \frac{\pi}{2}.$$

Numerical values for these vectors are provided in Tables I and II.

As described in Section III, pure translational trajectories can be designed based on sufficient conditions (14) and (15), which lead to the additional condition (23). Additionally, combined trajectories can be designed according to (35) and (36). If φ_j is defined as the angle between vector $\mathbf{Q}\mathbf{a}_j$ and vector $\mathbf{b}_j$, $\{\varphi_j\}_1^6$ will respect the equation

$$\varphi_j + \varphi_{j+3} = \pi, \quad j = 1, 2, 3$$

due to the symmetric arrangement of the cable attachment points. This leads in turn to

$$\mathbf{b}_j \times \mathbf{Q}\mathbf{a}_j + \mathbf{b}_{j+3} \times \mathbf{Q}\mathbf{a}_{j+3} = \mathbf{0}.$$

TABLE I
FIXED CABLE ATTACHMENT POINTS $\{\mathbf{b}_j\}_1^6$

j	$\mathbf{b}_j^T$ [m]			
1	[0.589	0.34	0	]
2	[0.000	0.68	0	]
3	[-0.589	0.34	0	]
4	[-0.589	-0.34	0	]
5	[0.000	-0.68	0	]
6	[0.589	-0.34	0	]

TABLE II
PLATFORM CABLE ATTACHMENT POINTS $\{\mathbf{a}_j\}_1^6$

j	$\mathbf{a}_j^T$ [m]			
1,4	[0.000	0.10	0.035	]
2,5	[0.087	-0.05	0.035	]
3,6	[-0.087	-0.05	0.035	]

With this constraint, the cable stiffnesses which respect condition (15) and (35) are obtained, namely

$$k_1 = k_4, \quad k_2 = k_5, \quad k_3 = k_6. \tag{64}$$

With $\{\mathbf{b}_j\}_1^6$ defined according to (62), conditions (23) and (36) are readily verified, since $\mathbf{w} = \mathbf{0}$. Additionally, for this *symmetric* mechanism, the resultant cable force during pure translational trajectories always points to the origin of the fixed frame O during the trajectories designed in Section III. For pure translational trajectories, the motion of the platform is governed by the linear dynamic equations (24).

B. Natural Trajectories

In Section III, natural trajectories were designed, which correspond to constant-stiffness springs in the passive equivalent system. For the specific architecture of the experimental prototype, positive constant stiffnesses $\{k_{sj}\}_1^6$ can be readily obtained from the constraints that define these trajectories, shown as follows for the cases of natural pure translation and natural combined motion.

1) Natural Pure Translation: Natural pure translation is simple harmonic motion, defined in (25), satisfying (15) and (29), with $\mathbf{Q} = \mathbf{1}$ and $H = 0$. Substituting the spring stiffnesses given in (64) and vectors $\{\mathbf{a}_j\}_1^6$ given in (63) into (29), one finds $d = 0$, which is a necessary condition for accomplishing these trajectories. Therefore, for natural pure translation, the cable attachment points on the experimental prototype are adjusted from $d = 0.035$ m as shown in Table II, to $d = 0$. When this condition is combined with the expressions for the natural frequencies given in (12) and (21), $\{k_{sj}\}_1^6$ are found to be

$$k_{s1} = k_{s2} = k_{s3} = k_{s4} = k_{s5} = k_{s6} = \frac{-mg}{6z_s}.$$

Additionally, the trajectory amplitude is unbounded, defined according to vectors $\mathbf{c}$ and $\mathbf{s}$ in (27).

2) Natural Combined Motion: Natural combined motion is a horizontal circular motion, with the platform orientation described by (20), (40), and (55). Using (50), (63), and (64), along with the equations $\mathbf{a}'_j = \mathbf{a}_j - \mathbf{d}$ and $\mathbf{d} = [0, 0, d]^T$, the relationship among $\{k_{sj}\}_1^6$ can be obtained. When this result is combined with the expressions for the natural frequencies given in (12) and (61), $\{k_{sj}\}_1^6$ are obtained as

$$k_{s1} = k_{s2} = k_{s3} = k_{s4} = k_{s5} = k_{s6} = \frac{-mg}{6(z_s + d\cos\theta_0)} \tag{65}$$

with the constraint of z_s given in (59). It is readily seen that $\{k_{sj}\}_1^6$ are always positive and constant. For such trajectories, the radius μ of the horizontal circle is not bounded. However, μ is subject to practical bounds due to its dependence on z_s and the tilt angle θ_0, given in (54) with $z = z_s$ and (20).

C. Extended Trajectories

Natural trajectories provide considerable insight into the behavior of the mechanism and can be described with a relatively simple mathematical formulation. However, these trajectories are unique and very restrictive. To permit trajectories with fewer restrictions, extended trajectories with *variable* spring stiffnesses are developed by applying a similar approach to that used for natural trajectories. Two examples are given, namely, elliptical translational linear trajectories and combined trajectories with both rotational and translational motion.

Transition trajectories proposed in [15] are applied to start from the state of rest and blend into the periodic trajectories. Using the algorithms presented in [23], it is guaranteed that no interference will occur among the cables or between the cables and the platform during the motion.

1) Pure Translation: Pure translational trajectories associated with variable stiffness springs can be described by the linear system (24) as long as condition (23) is satisfied. As usual, (14) and (15) must also be satisfied to yield the desired harmonic motion. Spring stiffnesses are again restricted according to (64), such that conditions (15) and (23) are satisfied. Based on (14) and (64), $\{k_j\}_1^6$ are found to be

$$k_j = \frac{m\omega_n^2}{6r(z+d)} k'_j \tag{66}$$

where

$$k'_1 = k'_4 = 2dy + rz, \quad k'_2 = k'_5 = d(\sqrt{3}x - y) + rz$$
$$k'_3 = k'_6 = -d(\sqrt{3}x + y) + rz.$$

Elliptical translational linear trajectories are designed to validate the feasibility of the trajectory planning method, defined as

$$\begin{aligned} x &= \mu_1 \cos\alpha \cos\omega_n t - \mu_2 \sin\alpha \sin\omega_n t \\ y &= \mu_1 \sin\alpha \cos\omega_n t + \mu_2 \cos\alpha \sin\omega_n t \\ z &= z_s + \mu_{zc} \cos\omega_n t \end{aligned} \tag{67}$$

where α is the angle between the x-axis and the major axis of the ellipse, z_s is the elevation of the horizontal elliptical trajectory, μ_1 is the major semiaxis, μ_2 is the minor semiaxis, μ_{zc} is the amplitude of z oscillations, ω_n is the natural frequency of translation, and t is time. This trajectory satisfies (25) with $\mathbf{p}_s = [0, 0, z_s]^T$, $\mathbf{c} = [\mu_1 \cos\alpha, \mu_1 \sin\alpha, \mu_{zc}]^T$, and $\mathbf{s} = [-\mu_2 \sin\alpha, \mu_2 \cos\alpha, 0]^T$.

Substituting the trajectory defined by (67) into (66), $\{k_j\}_1^6$ are obtained, namely

$$k_j = \frac{m\omega_n^2}{6r(z_s + d + \mu_{zc}\cos\omega_n t)} k'_j \tag{68}$$

where

$$\begin{aligned} k'_1 &= (2d\mu_1 \sin\alpha + r\mu_{zc})\cos\omega_n t \\ &\quad + 2d\mu_2 \cos\alpha \sin\omega_n t + rz_s \\ k'_2 &= (-2d\mu_1 \sin\alpha_2 + r\mu_{zc})\cos\omega_n t \\ &\quad - 2d\mu_2 \cos\alpha_2 \sin\omega_n t + rz_s \\ k'_3 &= (-2d\mu_1 \sin\alpha_3 + r\mu_{zc})\cos\omega_n t \\ &\quad - 2d\mu_2 \cos\alpha_3 \sin\omega_n t + rz_s \\ k'_4 &= k'_1, \quad k'_5 = k'_2, \quad k'_6 = k'_3 \end{aligned}$$

with $\alpha_2 = \alpha - \pi/3$ and $\alpha_3 = \alpha + \pi/3$.

If $z_s + d < -\mu_{zc}$, cables are always in tension as long as $k'_j < 0$. The bounds on trigonometric functions are applied to (68) to obtain the inequalities

$$\sqrt{(2d\mu_1 \sin\alpha + r\mu_{zc})^2 + 4d^2\mu_2^2 \cos^2\alpha} < -z_s r$$
$$\sqrt{(-2d\mu_1 \sin\alpha_2 + r\mu_{zc})^2 + 4d^2\mu_2^2 \cos^2\alpha_2} < -z_s r$$
$$\sqrt{(-2d\mu_1 \sin\alpha_3 + r\mu_{zc})^2 + 4d^2\mu_2^2 \cos^2\alpha_3} < -z_s r.$$

These are sufficient conditions to guarantee positive cable tensions. Furthermore, a single sufficient condition for satisfying these inequalities for any α is

$$\sqrt{4d^2(\mu_1^2 + \mu_2^2) + r^2\mu_{zc}^2} < -z_s r. \tag{69}$$

Based on this inequality, the amplitude is unbounded when $d = 0$, which is in agreement with the result found for natural pure translation, explored in Section III-A.

An example of elliptical translational motion is now provided. The following parameters are chosen: $\alpha = \pi/4$, $z_s = -1.5$ m, $\mu_1 = 1$ m, $\mu_2 = 0.6$ m, $\mu_{zc} = 0.4$ m, and $d = 0.035$ m. The frequency is, therefore, $\omega_n = \sqrt{-g/z_s} = 2.5573$ rad/s (24.4 r/min). The resulting motion is illustrated schematically in Fig. 7, including the transition phase. The cable tensions remain positive and continuous along the entire trajectory, as shown in Fig. 8.

2) Combined Motion: Combined motion is designed, which consists of a circular trajectory in the horizontal plane satisfying (52), with oscillations in z and variable ϕ. This is an extended case with respect to the natural combined motion that involves constant z and *dependent* μ, as shown in (54). For the extended case, μ is *independent* of z, and thus, (54) does not

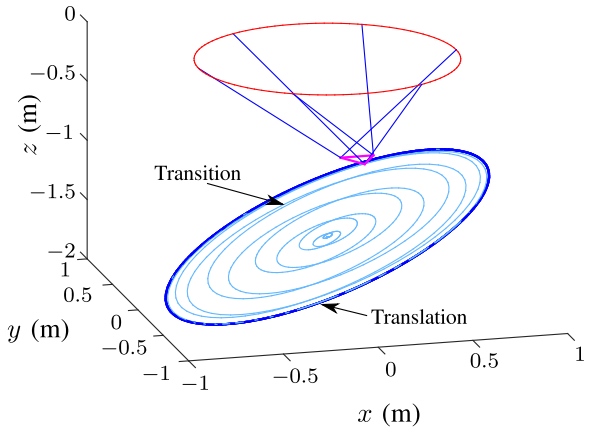

Fig. 7. Representation of the constant-orientation ellipse, including transitions.

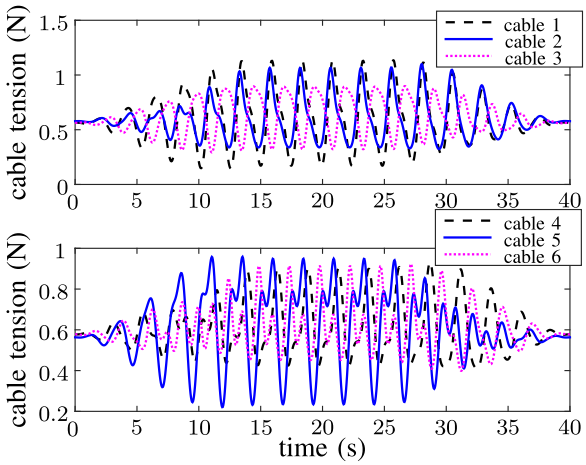

Fig. 8. Simulated cable tensions during the constant-orientation ellipse, including transitions.

apply. Using (46), (49), and (53), the left-hand side of (38) is simplified to

$$\mathbf{Q}(\mathbf{I}\dot{\boldsymbol{\omega}} + \boldsymbol{\omega} \times \mathbf{I}\boldsymbol{\omega}) - K\mathbf{p} \times \mathbf{Q}\mathbf{d} = c_{w1}\mathbf{s} \tag{70}$$

where

$$c_{w1} = \omega^2 c_I \sin\theta_0 - dK(z \sin\theta_0 + \mu \cos\theta_0). \tag{71}$$

Using the T&T angle convention introduced in Section III, and based on (38), (39), (64), and (70), k_1 and k_2 are eliminated according to

$$k_1 = k_3 + \frac{1}{2}k_{1s}, \quad k_2 = k_3 + \frac{1}{2}k_{2s} \tag{72}$$

where

$$k_{1s} = -\frac{\sqrt{3}(\sin\phi - \sqrt{3}\cos\phi)c_{w1}}{3\zeta r}$$

$$k_{2s} = -\frac{2\sqrt{3}\sin\phi c_{w1}}{3\zeta r}$$

with

$$\zeta = \mu \sin\theta_0 - z\cos\theta_0. \tag{73}$$

The scalar K is then found using (11), (64), and (72). Then, substituting (71) into (11), one has

$$K = 6k_3 - \frac{(\sqrt{3}\sin\phi - \cos\phi)c_{w1}}{\zeta r} > 0 \tag{74}$$

which gives

$$k_3 = \frac{1}{6}\left(K + \frac{c_{w1}}{\zeta r}(\sqrt{3}\sin\phi - \cos\phi)\right). \tag{75}$$

The substitution of the k_3 into (72) yields k_1 and k_2. Combining this result with (64), the spring stiffnesses are found to be

$$\begin{aligned} k_j &= \frac{K + h_j}{6} > 0, \quad j = 1, 2, 3 \\ k_4 &= k_1, \quad k_5 = k_2, \quad k_6 = k_3 \end{aligned} \tag{76}$$

where

$$\begin{aligned} h_1 &= -2\sqrt{7}\xi\cos(\phi + \delta_{\phi 1}) \\ h_2 &= -2\xi\cos\left(\phi - \frac{\pi}{3}\right) \\ h_3 &= -2\xi\cos\left(\phi + \frac{\pi}{3}\right). \end{aligned}$$

with

$$\xi = \frac{c_{w1}}{\zeta r}, \quad \delta_{\phi 1} = \operatorname{atan2}\left(\frac{\sqrt{3}}{\sqrt{7}}, \frac{2}{\sqrt{7}}\right).$$

With this result, the variable spring stiffnesses have been expressed as functions of the trajectory design parameters ω, μ, and θ_0, and the trajectory variables z and ϕ.

Consulting (73), for trajectories with $\theta_0 > 0$, $\mu > 0$, and $z < 0$, the inequality $\zeta > 0$ will be satisfied. The condition for $k_j > 0$ can be obtained from (76), which leads to the restriction

$$\zeta r > 2\sqrt{7}|\eta| \tag{77}$$

where $\eta = c_{w1}/K$.

It can be readily verified that if $c_{w1} = 0$, condition (77) is satisfied. Upon consulting (72) and (75), $c_{w1} = 0$ also makes the variable-stiffness equivalent passive equivalent system reduce to the constant-stiffness system described by (65).

Substituting (42), (63), and (76) into (39), one has

$$\mathbf{u} = \frac{c_{w1}}{\zeta}\begin{bmatrix} -\cos\theta_0 \sin\phi \\ \cos\theta_0 \cos\phi \\ \sin\theta_0 \end{bmatrix}. \tag{78}$$

Therefore, using (48), (53), and (78), (37) is expanded to

$$\begin{aligned} m\ddot{x} + K_n x &= 0 \\ m\ddot{y} + K_n y &= 0 \\ m\ddot{z} + Kz &= -Kd\cos\theta_0 - mg - \frac{c_{w1}\sin\theta_0}{\zeta} \end{aligned} \tag{79}$$

where

$$K_n = K\left(1 - \frac{d\sin\theta_0}{\mu}\right) + \frac{c_{w1}\cos\theta_0}{\mu\zeta} > 0. \tag{80}$$

Equations (53) and (55) are combined with the first two equations of (79) to produce

$$K_n = m\omega^2. \tag{81}$$

The last equation of (79) is then simplified by replacing the term c_{w1} with the value obtained from (80), producing

$$m\ddot{z} + Kz = -mg - \frac{\mu(m\omega^2 - K)\sin\theta_0 + dK}{\cos\theta_0} \tag{82}$$

which yields

$$K = \frac{N_K}{D_K} > 0 \tag{83}$$

where

$$N_K = -m(g + \ddot{z})\cos\theta_0 - m\mu\omega^2 \sin\theta_0$$
$$D_K = z\cos\theta_0 - \mu\sin\theta_0 + d.$$

In addition, (83) can be simplified to

$$K = \frac{m(g - \mu_{zs}\omega^2 \sin\omega t)\cos\theta_0 + m\mu\omega^2 \sin\theta_0}{\mu\sin\theta_0 - z\cos\theta_0 - d}$$
$$= m\omega^2 + K_1 > 0 \tag{84}$$

where

$$K_1 = \frac{N_{K1}}{D_{K1}}$$

with

$$N_{K1} = m(g + z_s\omega^2)\cos\theta_0 + m\omega^2 d, \quad D_{K1} = -D_K. \tag{85}$$

In summary, a combined trajectory with the platform translating circularly in the xy plane while oscillating in the z-direction and also changing orientation is feasible, since cable tensions are positive if conditions (77), (80), and (83) can be satisfied. It should be noted that z is not determined from the dynamic equations but left to be chosen to define the motion. One feasible trajectory can be defined by

$$x = \mu\cos\omega t, \quad y = \mu\sin\omega t, \quad z = z_s + \mu_{zs}\sin\omega t \tag{86}$$

and

$$\phi = \omega t - \pi/2, \quad \theta = \theta_0, \quad \sigma = 0. \tag{87}$$

Positioning along x, y, and z is, therefore, in phase, as was the case for elliptical translational trajectories. In fact, the positioning of the platform is very similar to that shown in Fig. 7, the distinguishing feature of the combined linear trajectories being that *the platform orientation is variable*. Additionally, the constraints

$$z_s < 0, \quad z_s + d < 0, \quad z_s + \mu_{zs} < 0 \tag{88}$$

are imposed.

The cables are always in tension during the trajectory if conditions (77), (80), (83), and (84) are met. Inequality (83) can be satisfied if

$$N_{K\max} = -m(g\cos\theta_0 + \mu\omega^2 \sin\theta_0 - \mu_{zs}\omega^2\cos\theta_0) < 0$$
$$D_{K\max} = (z_s + \mu_{zs})\cos\theta_0 - \mu\sin\theta_0 + d < 0 \tag{89}$$

while the minimum and maximum values of K can be readily determined from (84), namely

$$K_{\max} = m\omega^2 + K_{1\max}, \quad K_{\min} = m\omega^2 + K_{1\min}$$

where

$$K_{1\max} = \frac{N_{K1}}{\mu\sin\theta_0 - (z_s + \mu_{zs})\cos\theta_0 - d}$$

and

$$K_{1\min} = \frac{N_{K1}}{\mu\sin\theta_0 - (z_s - \mu_{zs})\cos\theta_0 - d}$$

for trajectories satisfying $N_{K1} > 0$. Moreover, one sufficient condition for satisfying (77) is

$$(\zeta r)_{\min} > 2\sqrt{7}\max(|\eta_1|, |\eta_2|) \tag{90}$$

where

$$|\eta_1| = |K_{\eta 1}\sin\theta_0 c_I\omega^2 - d(z_s - \mu_{zs})\sin\theta_0 - d\mu\cos\theta_0|$$
$$|\eta_2| = |K_{\eta 2}\sin\theta_0 c_I\omega^2 - d(z_s + \mu_{zs})\sin\theta_0 - d\mu\cos\theta_0|$$

with

$$c_I < 0, \quad K_{\eta 1} = \frac{1}{K_{\max}}, \text{ and } \quad K_{\eta 2} = \frac{1}{K_{\min}}.$$

Additionally, condition (80) can be satisfied if the numerator N_{Kn} of K_n is positive, since its denominator is also positive. $N_{Kn} > 0$ can be satisfied if

$$\{N_{Kn}\}_{\min} = \mu(\mu\sin\theta_0 - (z_s + \mu_{zs})\cos\theta_0 - d) + \frac{\omega^2\sin\theta_0\cos\theta_0 c_I}{K_{\max}} > 0 \tag{91}$$

is satisfied.

To demonstrate a combined trajectory with variable spring stiffnesses, an example is provided, which uses the following parameters: $z_s = -1.5$ m, $\mu = 1.2$ m, $\theta_0 = \pi/4$, $\mu_{zs} = 0.72$ m, and $d = 0.035$ m. The chosen frequency is $\omega = \sqrt{-g/z_s} = 2.5573$ rad/s (24.4 r/min) and the conditions (89)–(91) can be satisfied since

$$\{N_K\}_{\max} = -2.893\,\text{N}, \quad \{D_K\}_{\max} = -1.365\,\text{m}$$
$$\{\zeta r\}_{\min} = 0.14\,\text{m}^2, \quad 2\sqrt{7}\{|\eta|\}_{\max} = 0.119\,\text{m}^2$$
$$N_{K1} = m\omega^2 d > 0, \quad \{N_{Kn}\}_{\min} = 1.636\,\text{Nm}.$$

This trajectory guarantees continuous and positive cable tensions, as is confirmed in Fig. 9.

V. Discussion

The main contribution of this paper is the introduction of trajectory planning techniques that permit a 6-DOF cable robot to move its end effector *beyond* its static workspace in a controlled, predictable manner. Trajectories that involve variable stiffness equivalent springs and variable orientation are introduced, which is novel compared to previous work. The essential idea of the analytical method introduced is to find trajectories that are solutions to the dynamic equations. Another key insight is to divide the dynamic equations into two parts. Differential

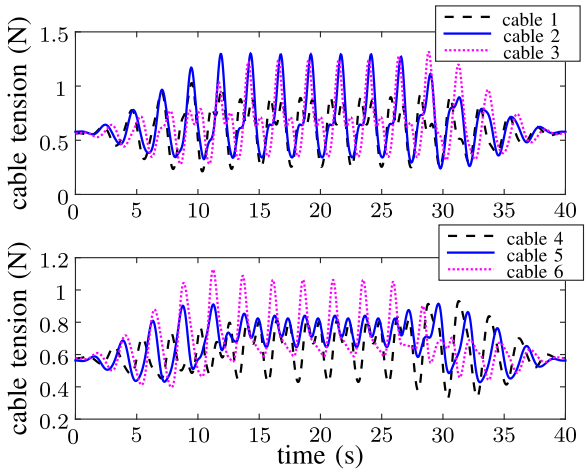

Fig. 9. Simulated cable tensions during an extended combined trajectory consisting of circular motion in x and y, oscillation in z, and variable orientation.

equation (24) can be integrated to yield periodic trajectories in pure translation, while (14), (15), and (23) are used as constraints on (24), ensuring that cable tensions remain positive. For combined motions, (37) and (38) are used to obtain trajectories, while (35) and (36) are constraints that must be respected, to ensure that cable tensions remain positive. This approach is more straightforward and systematic compared to previous techniques that involved *directly* using dynamic equations (9) and (10) [14], [15]. More importantly, it reveals the fundamental dynamic properties of CSPRs.

The six-actuator, 6-DOF cable robot is not an obvious choice for CSPR applications that require positioning and orientation of the platform. For example, it may be argued that a three- or four-cable positioning robot with actuators *on the platform* (e.g., the SkyCam [1]) is a better choice because it eliminates cable interference issues and can provide full rotational control. Obviously, this architecture is a better choice for some applications. However, the chosen six-actuator, 6-DOF architecture has many promising features, which were exploited in the applications described in [22] and [24]. First, the mechanism is fully parallel, with no actuators installed on the platform, thereby greatly simplifying the end-effector design and reducing its weight. Second, the chosen *crossing-cables* design resists off-center-of-mass forces and a carefully balanced end effector is, therefore, unnecessary.

The proposed periodic trajectories are good candidates for applications that do not require high accuracy, such as artistic performances [25] and entertainment [16]. Indeed, given the high velocities attained along the trajectories, high accuracy would be very difficult to achieve at all times. The 6-DOF experimental prototype described here was built using components similar to those used for a 3-DOF CSPR that positioned a point mass within a triangular-prism-shaped workspace of side length 9 m [26]. That system achieved a positioning error on the order of 1 cm [26], with platform speeds of up to 6 m/s. For the 6-DOF experimental prototype introduced in Section IV, proportional-derivative position control at 500 Hz is used to control the length of each cable. The cable positioning error based on the encoder feedback is approximately 4 mm for speeds of up to 3.58 m/s. Some additional cable length error results from cable wrapping variability.

A typical application of this study could involve hitting a point outside the static workspace, where some task is performed, such as taking a picture. In this case, the positioning accuracy matters most at this point and is not that important along the approach and recede segments of the trajectory. Given these considerations, a trajectory could be designed such that the end effector passes through the important point at zero speed, which maximizes the positioning accuracy there and also maximizes the time spent *near* this point.

VI. Conclusion

In this paper, the performance of dynamically feasible trajectories with 6-DOF CSPRs is investigated by exploring the fundamental properties of CSPRs. An equivalent passive mechanical system is introduced and a set of trajectories that can go beyond the static workspace are designed.

Several classes of dynamic trajectories are investigated for the 6-DOF mechanism. The first involves pure translation with constant orientation, while the second involves translation with the platform always facing toward the z-axis. For each of these cases, natural trajectories that correspond to constant-stiffness springs for the equivalent passive mechanical system are investigated, for which there is no restriction on the amplitude of oscillations. Third, variable-stiffness springs are explored to permit more general trajectories, such as oscillation in all three directions while also changing the platform orientation. For each type of trajectory, the positive-tension conditions are identified. An experimental prototype is used to demonstrate the trajectories, including transitions, as shown in the supplementary video file.

The main benefit of the proposed approach is that it can be used to plan dynamic trajectories that extend beyond the static workspace of the mechanism. Moreover, the basic trajectories introduced can be used as building blocks to synthesize more complex motion. Future work will involve extending the technique to permit the use of more general solutions to the dynamic equations, such as nontrigonometric solutions.

Acknowledgment

The authors would like to thank Mr. S. Foucault and Dr. D.-S. Vu for their help with the experimental validation.

References

[1] L. L. Cone, "Skycam: An aerial robotic camera system," *Byte*, vol. 10, no. 10, pp. 122–133, 1985.
[2] J. Albus, R. Bostelman, and N. Dagalakis, "The NIST robocrane," *J. Robot. Syst.*, vol. 10, no. 5, pp. 709–724, 1993.

[3] R. Nan and D. Li, "The five-hundred-meter aperture spherical radio telescope (FAST) project," in *Proc. IOP Conf. Series, Materials Sci. Eng.*, 2013, vol. 44, no. 1, pp. 12–22.
[4] O. Bohigas, M. Manubens, and L. Ros, "Planning wrench-feasible motions for cable-driven hexapods," *IEEE Trans. Robot.*, vol. 32, no. 2, pp. 442–451, Apr. 2016.
[5] E. Barnett and C. Gosselin, "Time-optimal trajectory planning of cable-driven parallel mechanisms for fully specified paths with G1-discontinuities," *J. Dyn. Syst., Meas., Control*, vol. 137, no. 7, pp. 071 007-1–071 007-12, 2015.
[6] H. R. Fahham and M. Farid, "Minimum-time trajectory planning of spatial cable-suspended robots along a specified path considering both tension and velocity constraints," *Eng. Optimization*, vol. 42, no. 4, pp. 387–402, 2010.
[7] M. Bamdad, "Time-energy optimal trajectory planning of cable-suspended manipulators," in *Cable-Driven Parallel Robots*, T. Bruckmann and A. Pott, Eds. Berlin, Germany: Springer, 2013, pp. 41–51.
[8] J. E. Bobrow, S. Dubowsky, and J. Gibson, "Time-optimal control of robotic manipulators along specified paths," *Int. J. Robot. Res.*, vol. 4, no. 3, pp. 3–17, 1985.
[9] K. Shin and N. McKay, "Minimum-time control of robotic manipulators with geometric path constraints," *IEEE Trans. Automat. Control*, vol. AC-30, no. 6, pp. 531–541, Jun. 1985.
[10] F. Pfeiffer and R. Johanni, "A concept for manipulator trajectory planning," *IEEE J. Robot. Autom.*, vol. RA-3, no. 2, pp. 115–123, Apr. 1987.
[11] M. Korayem and M. Bamdad, "Dynamic load-carrying capacity of cable-suspended parallel manipulators," *Int. J. Adv. Manuf. Technol.*, vol. 44, no. 7, pp. 829–840, 2009.
[12] M. Korayem, E. Davarzani, and M. Bamdad, "Optimal trajectory planning with the dynamic load carrying capacity of a flexible cable-suspended manipulator," *Scientia Iranica Trans. B, Mech. Eng.*, vol. 17, no. 4, pp. 315–326, 2010.
[13] M. H. Korayem, M. Bamdad, H. Tourajizadeh, A. H. Korayem, and S. Bayat, "Analytical design of optimal trajectory with dynamic load-carrying capacity for cable-suspended manipulator," *Int. J. Adv. Manuf. Technol.*, vol. 60, no. 1, pp. 317–327, 2012.
[14] C. Gosselin, P. Ren, and S. Foucault, "Dynamic trajectory planning of a two-dof cable-suspended parallel robot," in *Proc. IEEE Int. Conf. Robot. Autom.*, St. Paul, MN, USA, May 14–18, 2012, pp. 1476–1481.
[15] C. Gosselin, "Global planning of dynamically feasible trajectories for three-dof spatial cable-suspended parallel robots," in *Cable-Driven Parallel Robots*, T. Bruckmann and A. Pott, Eds. Berlin, Germany: Springer, 2013, pp. 3–22.
[16] V. Schmidt *et al.*, "Extending dynamic trajectories of cable-driven parallel robots as a novel robotic roller coaster," in *Proc. 41st Int. Symp. Robot.*, Messe München, Germany, Jun. 02–03, 2014, pp. 1–7.
[17] N. Zhang and W. Shang, "Dynamic trajectory planning of a 3-dof under-constrained cable-driven parallel robot," *Mechanism Mach. Theory*, vol. 98, pp. 21–35, 2016.
[18] N. Zhang, W. Shang, and S. Cong, "Geometry-based trajectory planning of a 3-3 cable-suspended parallel robot," *IEEE Trans. Robot.*, vol. 33, no. 2, pp. 484–491, Apr. 2017.
[19] X. Jiang and C. Gosselin, "Trajectory generation for three-degree-of-freedom cable-suspended parallel robots based on analytical integration of the dynamic equations," *J. Mechanisms Robot.*, vol. 8, no. 4, pp. 041 001–1–041 001–9, 2016.
[20] X. Jiang and C. Gosselin, "Dynamic point-to-point trajectory planning of a three-dof cable-suspended parallel robot," *IEEE Trans. Robot.*, vol. 32, no. 6, pp. 1550–1557, Dec. 2016.
[21] I. Bonev, D. Zlatanov, and C. Gosselin, "Advantages of the modified Euler angles in the design and control of PKMs," in *Proc. Parallel Kinematic Mach. Int. Conf.*, Chemnitz, Germany, Apr. 23–25, 2002, pp. 171–188.
[22] C. M. Gosselin and S. Bouchard, "A gravity-powered mechanism for extending the workspace of a cable-driven parallel mechanism: Application to the appearance modelling of objects," *Int. J. Autom. Technol.*, vol. 4, pp. 372–379, 2010.
[23] S. Perreault, P. Cardou, C. M. Gosselin, and M. J.-D. Otis, "Geometric determination of the interference-free constant-orientation workspace of parallel cable-driven mechanisms," *J. Mechanisms Robot.*, vol. 2, no. 3, pp. 031 016-1–031 016-9, 2010.
[24] E. Barnett and C. Gosselin, "Large-scale 3D printing with a cable-suspended robot," *Additive Manuf.*, vol. 7, pp. 27–44, 2015.
[25] P. Tempel, F. Schnelle, A. Pott, and P. Eberhard, "Design and programming for cable-driven parallel robots in the German Pavilion at the EXPO 2015," *Machines*, vol. 3, no. 3, pp. 223–241, 2015.
[26] C. Gosselin and S. Foucault, "Experimental determination of the accuracy of a three-dof cable suspended parallel robot performing dynamic trajectories," in *Cable-Driven Parallel Robots*, A. Pott and T. Bruckmann, Eds. Berlin, Germany: Springer, 2015, pp. 101–112.

Xiaoling Jiang received the B.Eng. and M.Eng. degrees in mechanical engineering from Huaqiao University, Xiamen, China, in 2009 and 2012, respectively, and the Ph.D. degree in mechanical engineering from Laval University, Québec, QC, Canada, in 2017.

She is currently with the Faculty of Mechanical Engineering and Automation, Zhejiang Sci-Tech University, Hangzhou, China. She received a Doctorate Scholarship from the China Scholarship Council (CSC) from 2012 to 2016. Her research interests include dynamic trajectory planning and synthesis of cable-suspended parallel robots.

Dr. Jiang is a member of the American Society of Mechanical Engineers.

Eric Barnett received the B.Eng. and Ph.D. degrees in mechanical engineering from McGill University, Montreal, QC, Canada, in 2007 and 2012, respectively.

He is a Research Associate with the Robotics Laboratory, Department of Mechanical Engineering, Laval University, Québec, QC, Canada. He is also currently with Robotiq, Lévis, QC, Canada. His research interests include additive manufacturing, trajectory planning, and human–robot interaction.

Clément Gosselin (S'87–M'90–SM'10–F'13) received the B. Eng. degree in mechanical engineering from Université de Sherbrooke, Sherbrooke, QC, Canada, in 1985 and the Ph.D. degree in mechanical engineering from McGill University, Montréal, QC, in 1988.

He was a Postdoctoral Fellow with INRIA, Sophia-Antipolis, France, in 1988–1989. In 1989, he joined the Department of Mechanical Engineering, *Université Laval*, Québec, QC, where he has been a Full Professor since 1997. He was a Visiting Researcher with RWTH Aachen University, Aachen, Germany, in 1995; with University of Victoria, Victoria, Canada, in 1996; and with the IRCCyN, Nantes, France in 1999. His research interests include kinematics, dynamics and control of robotic mechanical systems with a particular emphasis on the mechanics of grasping, the kinematics and dynamics of parallel manipulators, and the development of human-friendly robots. His work in the aforementioned areas has been the subject of numerous publications in international journals and conferences as well as of several patents and two books. He has been directing many research initiatives, including collaborations with several Canadian and foreign high-technology companies and he has trained more than 100 graduate students.

Dr. Gosselin is an Associate Editor of IEEE ROBOTICS AND AUTOMATION LETTERS and of *ASME Journal of Mechanisms and Robotics*. He has held a Canada Research Chair in Robotics and Mechatronics since January 2001. He was the recipient of several awards including the ASME DED Mechanisms and Robotics Committee Award in 2008 and the ASME Machine Design Award in 2013. He was appointed Officer of the Order of Canada in 2010 for contributions to research in parallel mechanisms and underactuated systems. He is a Fellow of the American Society of Mechanical Engineers and the Royal Society of Canada.